

## **Continuous-flow synthesis of mesoporous SBA-15**

### Author

Parlett, Christopher MA, Arandiyán, Hamidreza, Durndell, Lee J, Isaacs, Mark A, Lopez, Antonio Torres, Wong, Roong J, Wilson, Karen, Lee, Adam F

### Published

2022

### Journal Title

Microporous and Mesoporous Materials

### Version

Accepted Manuscript (AM)

### DOI

[10.1016/j.micromeso.2021.111535](https://doi.org/10.1016/j.micromeso.2021.111535)

### Rights statement

© 2021. This manuscript version is made available under the CC-BY-NC-ND 4.0 license <https://creativecommons.org/licenses/by-nc-nd/4.0/>

### Downloaded from

<https://hdl.handle.net/10072/432892>

### Funder(s)

ARC

### Grant identifier(s)

DP200100313

### Griffith Research Online

<https://research-repository.griffith.edu.au>

# Continuous-flow synthesis of mesoporous SBA-15

Christopher M.A. Parlett,<sup>\*a,b,c</sup> Hamidreza Arandiyani,<sup>d</sup> Lee J. Durndell,<sup>e</sup> Mark A. Isaacs,<sup>f,g</sup> Antonio Torres Lopez,<sup>a,h</sup>  
Roong J. Wong,<sup>i</sup> Karen Wilson<sup>d</sup> and Adam F. Lee<sup>\*d</sup>

<sup>a</sup>Department of Chemical Engineering and Analytical Science, University of Manchester, Manchester M13 9PL, UK.

<sup>b</sup>University of Manchester at Harwell, Diamond Light Source, Rutherford Appleton Laboratory, Didcot, Oxfordshire, OX11 0DE, UK.

<sup>c</sup>Diamond Light Source, Rutherford Appleton Laboratory, Didcot, Oxfordshire, OX11 0DE, UK.

<sup>d</sup>Centre for Advanced Materials and Industrial Chemistry (CAMIC), RMIT University, Melbourne VIC 3000, Australia.

<sup>e</sup>School of Geography, Earth and Environmental Sciences, Plymouth University, Plymouth, PL4 8AA, UK.

<sup>f</sup>Department of Chemistry, University College London, London, WC1E 6BT, UK.

<sup>g</sup>HarwellXPS, Research Complex at Harwell, Rutherford Appleton Laboratory, Didcot, Oxfordshire, OX11 0DE, UK.

<sup>h</sup>UK Catalysis Hub, Research Complex at Harwell, Rutherford Appleton Laboratory, Harwell, Oxfordshire OX11 0FA, UK

<sup>i</sup>School of Chemical and Biomedical Engineering, Nanyang Technology University, Singapore 637459, Singapore.

Corresponding authors: [christopher.parlett@manchester.ac.uk](mailto:christopher.parlett@manchester.ac.uk); [adam.lee2@rmit.edu.au](mailto:adam.lee2@rmit.edu.au)

## Abstract

Ordered mesoporous silicas are widely used in separation science and catalysis, however, their slow batch synthesis is a barrier to scale-up and new applications. SBA-15 is one of the most extensively studied and commercially available mesoporous silicas, whose textural properties can be readily tuned through judicious choice of synthesis conditions. Here we demonstrate the continuous flow synthesis of SBA-15 in high yield at 80 °C using a simple tube reactor without any mixing device. The resulting SBA-15 exhibits excellent textural properties, with a BET surface area of 566 m<sup>2</sup>.g<sup>-1</sup> and ordered 5.1 nm mesopore channels in a *p6mm* arrangement, akin to those from conventional batch synthesis, but with far higher productivity than previously reported in batch or flow (5.3 g.L<sup>-1</sup>.h<sup>-1</sup> versus 0.4 and 0.6 g.L<sup>-1</sup>.h<sup>-1</sup> respectively).

Keywords: mesoporous silica; continuous flow; SBA-15; material synthesis

## 1. Introduction

Since their first synthesis by the Mobile Oil Corporation in 1992,<sup>1</sup> ordered mesoporous silica (OMS) has stimulated intensive academic research and commercial application<sup>2</sup> in areas spanning separation science,<sup>3</sup> drug delivery,<sup>4</sup> catalysis,<sup>5</sup> and nanofabrication<sup>6</sup> due to their desirable and tunable physicochemical properties. Subsequent development of the Santa Barbara Amorphous (SBA) family of larger pore OMS, through the use of non-ionic block copolymers, afforded thicker-walled materials with improved hydrothermal stability.<sup>7</sup> Of these, SBA-15 is the most widely studied, comprising a hexagonal close-packed arrangement of typically 5 nm cylindrical mesopores (with expansion up to 30 nm possible using poragens<sup>7</sup>). Previous reports have explored the mechanism of SBA-15 formation,<sup>8, 9</sup> mesopore expansion,<sup>10</sup> morphology control,<sup>11</sup> and the nature of complementary microporosity.<sup>12</sup> Applications of SBA-15 include as catalyst supports,<sup>13, 14</sup>

stationary phase for liquid chromatography,<sup>3, 15</sup> drug delivery scaffold,<sup>4, 16</sup> frameworks for the immobilisation of antimicrobial agents,<sup>17, 18</sup> and gas adsorption and/or separation.<sup>19, 20</sup>

The production of OMS is dominated by batchwise synthesis, hindering industrial scale-up due to associated slow mass transport, poor temperature regulation, and regular start-up/shutdown procedures, which result in relatively low yields and long (~24 h) preparation times. The recent upsurge in continuous flow synthesis, in part due to its green credentials and potential for new chemical transformations,<sup>21</sup> has led to its exploitation in the manufacture of natural products,<sup>22</sup> catalysis,<sup>23</sup> and the synthesis of nanoparticles<sup>24</sup> and to a lesser degree porous solids. Self-assembly of crystalline metal-organic frameworks (MOFs) can be rapid and is amenable to continuous-flow production with residence times on the order of minutes.<sup>25</sup> Ultra-fast synthesis of zeolites, including industrially important ZSM-5 and SAPO-34, has also been achieved in continuous flow by rapid crystallisation at temperatures >250 °C,<sup>26</sup> with high space-time yields reaching ~7,000 kg/m<sup>3</sup>.h (comparable to batch synthesis). Despite such benefits, there are few reports on the flow synthesis of mesoporous silicas in flow reactors.<sup>27-31</sup> Ng et al. reported proof-of-concept flow production of OMS solid and hollow mesoscopic particles;<sup>32</sup> particle size and morphology was a function of liquid and gas velocities, and interdigital micromixer design. However, silica yields were low (15%) and particle size distributions broad (e.g. 460 ± 110 nm) unless very small OMS particles were prepared. Microfluidic devices also enable the synthesis of hollow (disordered) mesoporous silica microspheres, by combining water-in-oil emulsion droplets with a Pluronic non-ionic surfactant.<sup>33</sup>

Cationic surfactant templating has also been utilised to introduce porosity into silica nanospheres prepared under continuous flow, with dimensions spanning the nanometre to micron range,<sup>30, 32, 34, 35</sup> and morphologies varying from uniform mesoporous particles<sup>30, 34</sup> to solid core-porous shell<sup>32</sup> and hollow core-shell structures.<sup>30, 35</sup> However, the majority of such silica nanospheres exhibit disordered mesopores, with only the flow synthesis of ordered MCM-41 claimed (albeit without supporting diffraction or electron microscopy).<sup>34</sup> Control over silica morphology has also been demonstrated using microfluidic approaches, in which different reactants and concentrations yielded ordered mesoporous ellipsoids,<sup>36</sup> or disordered mesoporous fibres<sup>29</sup> or rippled surface sheets.<sup>37</sup> Microwave hydrothermal synthesis is commonly conducted batchwise, but has been extended to the flow synthesis of silica nanopowders,<sup>38</sup> albeit on a small scale and producing moderate surface area materials. Nevertheless, the extremely fast crystallisation kinetics associated with microwave hydrothermal synthesis can dramatically reduce requisite processing times.<sup>39</sup> Fei et al. recently reported the continuous synthesis of monodisperse silica microspheres (with sizes >1 µm)<sup>40</sup> through a Stöber method;<sup>41</sup> cetyltrimethylammonium bromide addition helped prevent blockage of the flow reactor and improve dispersity of the resulting silica microspheres.

COK-12 is a hexagonally ordered mesoporous silica<sup>42</sup> with a similar pore diameter and space group to SBA-15, reflecting the common Pluronic P123 surfactant, but which spontaneously forms at room temperature and near neutral pH; it has been prepared under continuous flow<sup>43</sup> at short residence times (~0.5 min), facilitated by almost instantaneous precipitation of the templated silica, albeit with a low productivity of 0.5 g.L<sup>-1</sup>.h<sup>-1</sup>. Colmenares et al. synthesised a monolithic COK-12 silica, with 5-6 nm hexagonal close-packed cylindrical pores, by continuous flow synthesis using an acidic medium,<sup>44</sup> achieving a production capacity of 330 g/run. Continuous synthesis of SBA-15 (characterised by 2D hexagonal mesopores) was demonstrated using a dropwise flow reactor, with paraffin oil as a carrier/continuous phase to disperse aqueous precursors. This approach necessitated an active mixer and two heating units, increasing overall process complexity, and was hampered by fracturing of embryonic 2D hexagonal silica particles by the active mixer, or frequent clogging of syringes due to premature silica particle formation when TEOS and P123 precursors were premixed with HCl.<sup>27</sup> Flow synthesis of SBA-15 under ambient conditions is hindered by slow crystallisation, prompting the application of a vortex fluidic reactor

to improve mass transport and reaction kinetics.<sup>31</sup> However, the resulting silica yield was only ~67.5 %, and the multistep synthesis combined with sample drying pre-calcination limited SBA-15 productivity to only 0.6 g.L<sup>-1</sup>.h<sup>-1</sup>; scale-up of such technology is also challenging. Here we report the continuous flow production of SBA-15 within a simple, heated tubular reactor, with optimal conditions enabling significantly reduced residence times and enhanced productivity of 5.3 g.L<sup>-1</sup>.h<sup>-1</sup>.

## 2. Experimental

### 2.1 Materials synthesis

SBA-15 was synthesised using a bespoke tubular reactor (**Figure 1**) comprising 300 mm × 5.5 mm i.d. PTFE tubing (~7.1 mL internal volume) placed within a shroud of 12.7 mm o.d. stainless steel tube, itself wrapped with heating tape and a K-type thermocouple in contact with the exterior of the steel tube. The latter provided temperature regulation from room temperature up to 100 ±2 °C. An acidic, aqueous surfactant solution comprising 20 g of Pluronic P123 (Sigma Aldrich, average M<sub>n</sub> ~5,800), 635 mL of deionised H<sub>2</sub>O and 97 mL of 12 M HCl (Sigma Aldrich) was stirred at room temperature for 1 h to ensure complete surfactant dissolution and then fed by a Watson Marlow 120U/DM2 peristaltic pump at 0.52 mL.min<sup>-1</sup> into the PTFE reactor held at 80 °C via a 6.4 mm PTFE Swagelok T-piece into which pure tetramethyl orthosilicate (TMOS, Sigma Aldrich, 98 %) was co-fed at 0.019 mL.min<sup>-1</sup> by a Cole-Palmer syringe pump. Slurry exiting the PTFE reactor was collected over a 1 h period in a downstream 30 mL Buchner funnel and immediately subject to vacuum filtration (~0.1 bar) to isolate the solid product. Immediately the surfactant template was removed by calcination at 550 °C for 6 h (ramp rate 1 °C.min<sup>-1</sup>) to yield the final material designated SBA-15(flow). Note that this thermal processing is sufficient to fully remove the organic template from conventionally prepared SBA-15,<sup>45</sup> and indeed the resulting SBA-15(flow) was a bright, white powder indicative of complete P123 combustion. A control sample was prepared by literature batchwise synthesis.<sup>7</sup> 2.0 g of Pluronic P123 was dissolved in 15.1 mL deionised H<sub>2</sub>O and 58.3 mL 2 M HCl under stirring at 35 °C for 1 h. 3.1 mL TMOS was added and left for 20 h with agitation. The sol-gel was hydrothermally treated under sealed conditions for 24 h at 80 °C without agitation. The solid was filtered, washed with 200 mL deionised H<sub>2</sub>O and dried at room temp before calcination at 550 °C for 6 h in air (ramp rate 1 °C.min<sup>-1</sup>). The material was designated SBA-15(batch).

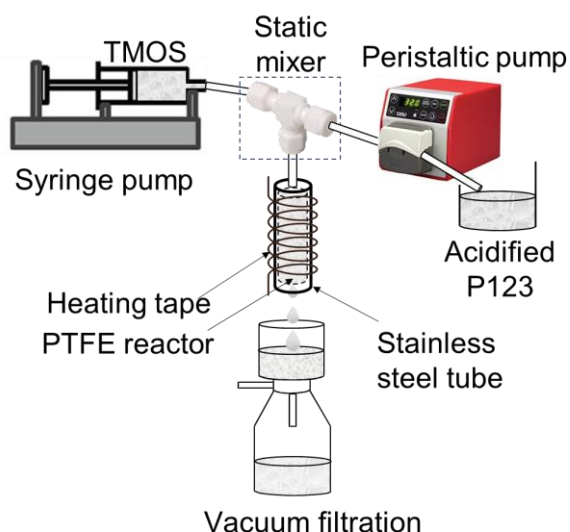


**Figure 1.** Schematic of apparatus for continuous flow synthesis of SBA-15.

## 2.2 Materials characterisation

Low angle powder X-ray diffraction (XRD) patterns were collected on a Bruker D8 Advance Diffractometer with a LynxEye high-speed strip detector using Cu  $K_{\alpha}$  (1.54 Å) radiation, Ni filter and calibrated to quartz. Low angle data were collected between  $2\theta = 0.45\text{--}6^{\circ}$  with a step size of  $0.01^{\circ}$  at  $0.0125^{\circ} \text{ s}^{-1}$ . Nitrogen adsorption-desorption isotherms were recorded on a Quantachrome Nova 4200e porosimeter with data analysis employing Novawin v11.3 software. Samples were degassed at  $150^{\circ}\text{C}$  for 4 h prior to analysis by nitrogen adsorption at  $-196^{\circ}\text{C}$ . BET surface areas were calculated over the range  $P/P_0 = 0.05\text{--}0.2$  where a linear relationship was maintained, pore size distributions were calculated using the BJH equation applied to the desorption branch of the isotherm and NLDFIT fit to a N2 at 77 K on silica with cylindrical pores model, and microporosity was assessed by the t-plot method over the range  $P/P_0 = 0.2\text{--}0.5$ . High-resolution bright-field scanning transmission electron microscopy (STEM) images were obtained on an aberration-corrected JEOL 2100-F microscope operated at 200 kV, with image processing using ImageJ 1.41 software. Samples were dispersed in methanol and drop cast on 200-mesh carbon coated copper grids and dried under ambient conditions. Scanning electron microscopy (SEM) images were acquired using an FEI Verios 460L FEGSEM operating at 0.5kV with a 2kV stage bias, with powder samples deposited onto carbon tape and mounted onto SEM stubs.

## 3. Results and discussion

Successful flow synthesis of ordered SBA-15 mesoporous silica using a simple tube reactor was demonstrated by porosimetry, XRD and electron microscopy. Nitrogen adsorption-desorption of SBA-15(flow) evidenced the expected type IV(a) isotherm with H1 hysteresis loop (**Figure 2a**),<sup>46</sup> similar to that of the conventional SBA-15(batch) material. Corresponding BJH pore-size distributions (**Figure S1**) revealed mono-modal mesopores with mean diameters of 5.1 nm for both flow and batch synthesised silicas, although the BET surface area of the former was approximately 62 % of the latter largely due to loss of complimentary microporosity (**Table 1**). Low angle XRD patterns of flow and batch synthesised silicas (**Figure 2b**) exhibit peaks at  $2\theta = 0.9^{\circ}$ ,  $1.6^{\circ}$  and  $1.9^{\circ}$  corresponding to (100), (110) and (200) reflections characteristic of the  $p6mm$  arrangement of hexagonal mesoporous channels in SBA-15. Corresponding unit cells determined from the  $d_{10}$  reflections were 8.8 nm and 9.0 nm for flow and batchwise synthesis respectively. SEM reveals similar rod-like particle morphologies (**Figure 2c**) for SBA-15(flow) and SBA-15(batch) consistent with the literature, although only partial assembly into larger alfalfa-like macrostructures was observed for the flow synthesised silica, akin to reports for SBA-15 synthesised batchwise without agitation.<sup>47</sup> High-resolution bright-field STEM confirmed a  $p6mm$  arrangement of hexagonal close-packed mesopores for both silicas (**Figure 2c**) and similar mesopore domain sizes extending  $>500$  nm (**Figure S2**). Overall, there was excellent reproducibility between SBA-15 synthesised in batch and continuous flow using a tubular reactor and simple static mixer, with the principal difference being a lower surface area due to reduced microporosity akin to SBA-15 prepared by true liquid crystal templating.<sup>48</sup> The isolated yield of SBA-15(flow) of 79 % is slightly lower than our and literature reports for batchwise synthesis of  $\sim 95\%$ ,<sup>45</sup> but surpasses that for more complex vortex fluidic reactors.<sup>31</sup> The space-time yield of SBA-15 using our tube reactor was  $5.3 \text{ g.L}^{-1}.\text{h}^{-1}$  represents a 16-fold increase in productivity relative to conventional bulk SBA-15 ( $0.4 \text{ g.L}^{-1}.\text{h}^{-1}$ ) synthesis and significantly exceeds previous reports for the continuous synthesis of SBA-15 or COK-12 ( $0.6$  and  $0.5 \text{ g.L}^{-1}.\text{h}^{-1}$  respectively).<sup>31, 43</sup> Note that SBA-15(flow) and SBA-15(batch) underwent identical high temperature calcination prior to their characterisation, and hence appear to possess similar thermal stability.

**Table 1.** Textural properties of SBA-15(flow) versus SBA-15(batch).

| Sample                                      | BET surface area <sup>a</sup> / m <sup>2</sup> .g <sup>-1</sup> | Micropore area <sup>b</sup> / m <sup>2</sup> .g <sup>-1</sup> | Pore volume <sup>a</sup> / cm <sup>3</sup> .g <sup>-1</sup> | BJH pore diameter <sup>a</sup> / nm | NLDFT pore diameter / nm <sup>a</sup> | d <sub>10</sub> <sup>b</sup> / nm | Unit cell <sup>b</sup> / nm |
|---------------------------------------------|-----------------------------------------------------------------|---------------------------------------------------------------|-------------------------------------------------------------|-------------------------------------|---------------------------------------|-----------------------------------|-----------------------------|
| SBA-15(batch)                               | 910                                                             | 360                                                           | 0.96                                                        | 5.1                                 | 6.6                                   | 9.0                               | 10.3                        |
| SBA-15(flow) 1 <sup>st</sup> h <sup>c</sup> | 566                                                             | 150                                                           | 0.81                                                        | 5.1                                 | 6.3                                   | 8.8                               | 10.2                        |
| SBA-15(flow) 2 <sup>nd</sup> h <sup>c</sup> | 569                                                             | 157                                                           | 0.73                                                        | 5.4                                 | 6.7                                   | 8.8                               | 10.2                        |
| SBA-15(flow) 3 <sup>rd</sup> h <sup>c</sup> | 520                                                             | 184                                                           | 0.54                                                        | 5.1                                 | 6.5                                   | 8.7                               | 10.1                        |
| SBA-15(flow) 70 °C                          | 479                                                             | 192                                                           | 0.54                                                        | 5.7                                 | 7.0                                   | 8.9                               | 10.3                        |
| SBA-15(flow) 60 °C                          | 420                                                             | 137                                                           | 0.49                                                        | 5.8                                 | 7.0                                   | 8.7                               | 10.1                        |
| SBA-15(flow) 50 °C                          | 365                                                             | 45                                                            | 0.54                                                        | 5.7                                 | 7.0                                   | 8.7                               | 10.1                        |
| SBA-15(flow) 6.5 min                        | 534                                                             | 256                                                           | 0.47                                                        | 3.9                                 | 5.1                                   | 8.7                               | 10.1                        |
| SBA-15(flow) 4.3 min                        | 495                                                             | 266                                                           | 0.39                                                        | 3.9                                 | 5.2                                   | 8.8                               | 10.2                        |
| SBA-15(flow)-HT <sup>d</sup>                | 735                                                             | 310                                                           | 0.87                                                        | 6.0                                 | 7.9                                   | 10.5                              | 12.1                        |

<sup>a</sup>N<sub>2</sub> porosimetry; <sup>b</sup>Low angle XRD; <sup>c</sup>Standard conditions: 80 °C and 13 min residence time; <sup>d</sup>Hydrothermal treatment

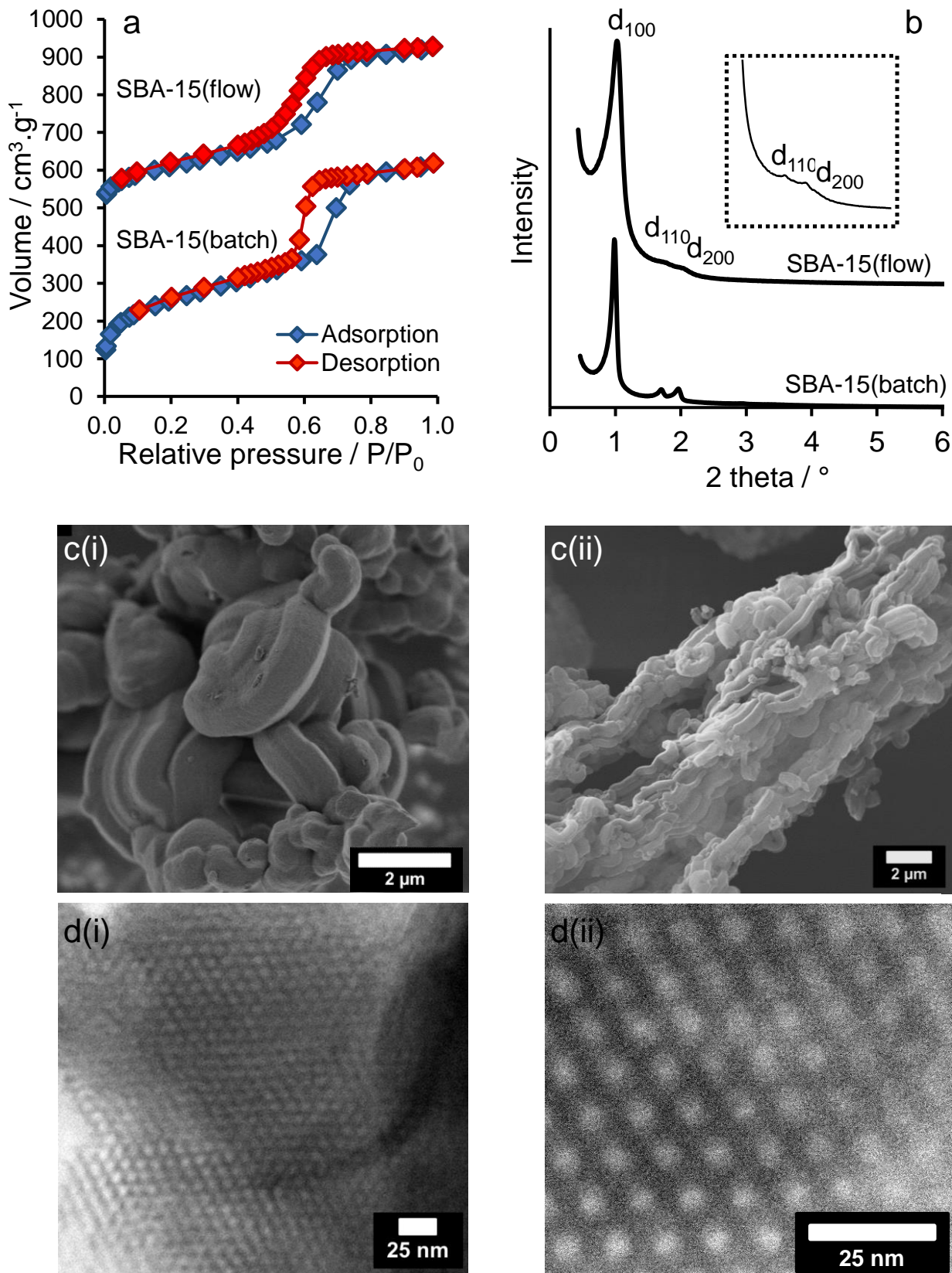


**Figure 2.** (a) N<sub>2</sub> adsorption-desorption isotherms, (b) Low angle XRD patterns (inset highlighting d<sub>110</sub> and d<sub>200</sub> peaks), and corresponding (c) SEM and (d) bright-field STEM images of (i) SBA-15(flow) and (ii) SBA-15(batch). XRD patterns and isotherms offset for clarity.

Given the relative ease and success of our continuous SBA-15 synthesis, the stability of flow production was evaluated over extended runs. The ordered mesopore architecture was preserved over 3 h continuous operation, evidenced by STEM

(**Figure 2**), low angle XRD and nitrogen porosimetry (**Figure S3**) wherein only a small decrease in surface area, total pore volume and mesopore diameter were observed (**Table 1**), although a small drop (18 %) in isolated yield was observed with increasing reaction time. The modest change in textural properties and silica yield likely reflect fouling of the reactor walls by viscous, partially condensed, organic-inorganic mesophases, thereby decreasing the true reactor volume and shortening the residence time experienced by reagents during the third hour of reaction. This would explain the similarity of textural properties for SBA-15(flow) obtained after 3 h reaction with a nominal residence time of 13 min with those of SBA-15(flow) obtained after 1 h at a residence time of 6.5 min. Scale-up could mitigate such fouling through the use of wide bore tubing (to minimise wall effects relative to the reactor volume) and the introduction of static mixers within the tubing (to promote turbulent flow and hence eliminate a laminar boundary layer at the reactor walls, which will improve heat transfer and minimise fouling for low reagent velocities<sup>49, 50</sup>). Future studies will explore the use of PTFE oscillatory baffled reactors<sup>51</sup> to optimise the reactor configuration for reproducible, large scale SBA-15 flow synthesis.

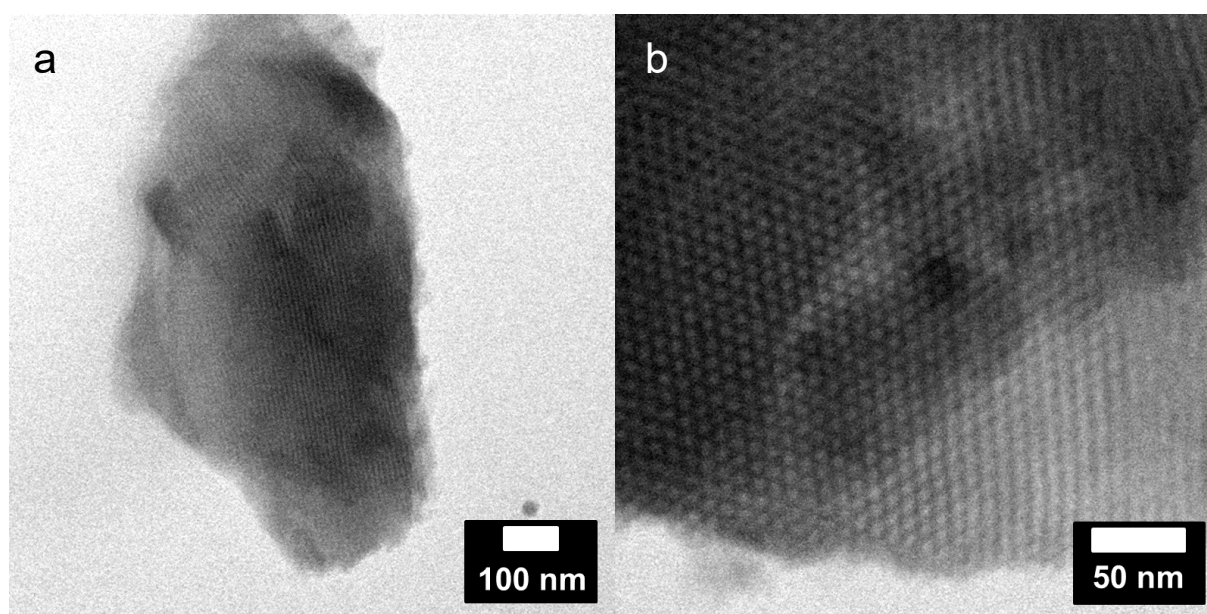


**Figure 2.** (a-b) STEM images of SBA-15(flow) collected during the third hour of continuous operation highlighting preservation of hexagonal close packed cylindrical mesopores channels.

Selection of the appropriate reaction temperature and residence time is critical to a successful flow synthesis. Although ordered mesopores and a modest surface area were retained at reaction temperatures as low as 50 °C (**Figure S4** and **Table 1**), lower temperatures significantly decreased the SBA-15 yield (**Figure 3**).

Residence time within the reactor tube exerted a stronger influence on textural properties, with shorter times resulting in a significant loss of mesopore order, apparent from low angle XRD and STEM (**Figure S5-S6**), and particle size shrinkage with a more spherical morphology from SEM (**Figure S7**), which are accompanied by a slight decrease in surface area, pore volume and mesopore diameter (**Table 1**). Nitrogen porosimetry also revealed a transition to H2 type hysteresis (**Figure S5**) indicative of ink bottle pore opening and spherical pores. Such a transition is representative of a close alignment with the batch synthesis growth mechanism in which spherical surfactant micelles are transformed via interaction with silica oligomers into cylindrical pore architectures via a wormlike thread intermediate.<sup>8, 9</sup> Short residence times favour silicas constructed of assemblies of disordered spherical pores, while intermediate residence times yield composite materials with mixed spherical and rod morphology and a bimodal distribution of mesopores.

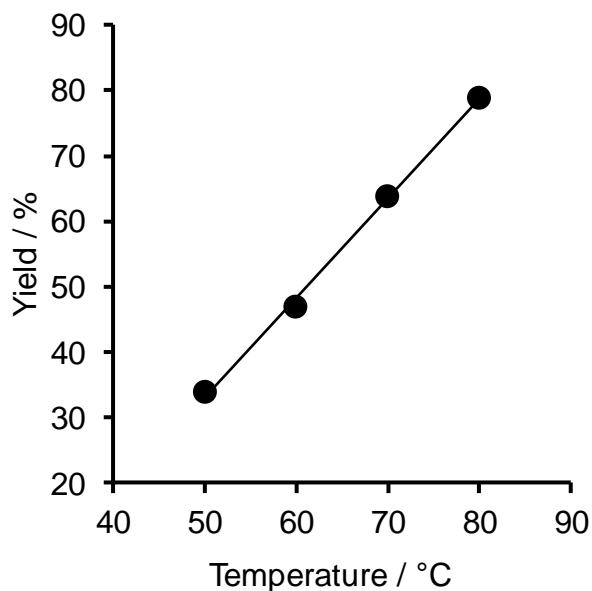


**Figure 3.** Temperature-dependent SBA-15(flow) yield.

Akin to conventional SBA-15 prepared via the route of Zhao et al.,<sup>45</sup> our calcined SBA-15(flow) shows excellent hydrothermal stability after 24 h immersion in boiling water (**Figure S8**). Retention of the parent silica hexagonal pore architecture and textural properties was confirmed by TEM and N<sub>2</sub> porosimetry; the resulting BET surface area (518 m<sup>2</sup> g<sup>-1</sup>) and BJH average pore diameter (5.1 nm) were similar to the as-prepared SBA-15(flow) material.

The textural properties of flow synthesised SBA-15 (prepared under our acidic conditions) could be enhanced by incorporating a 16 h hydrothermal treatment of the unwashed isolated silica at 80 °C prior calcination (**Table 1**). Such protocols can increase long-range order in mesoporous silica prepared under basic conditions.<sup>52</sup> This additional hydrothermal treatment increased both the BET and micropore surface areas and total pore volume closer to those of SBA-15(batch), and also expanded the unit cell and mean mesopore diameter (**Figure S9**). Hydrothermal swelling of porous silica is well known for batch-synthesised SBA-15,<sup>53</sup> wherein surface areas increase through greater penetration of the polyethene oxide groups of Pluronic P123 into nascent silica walls. Evaporation-induced self-assembly of mesoporous silica is similarly influenced by post-synthesis processing.<sup>2</sup> Despite improving the textural properties, hydrothermal treatment of SBA-15(flow) did not promote the assembly of mesoporous silica rods (**Figure S10**) into the straw-like macrostructures typical of SBA-15(batch) (**Figure 1cii**). Furthermore, its inclusion diminishes productivity to 0.6 g.L<sup>-1</sup>.h<sup>-1</sup> due solely to increased total reaction time. Hydrothermal treatment is not expected to significantly influence the SBA-15 yield, since any mass losses would solely arise from the filtration recovery step. Indeed, the yield of SBA-15(flow)-HT was 78 %, almost identical to that obtained for SBA-15(flow) without hydrothermal treatment.

#### 4. Conclusions

Continuous flow synthesis of a highly ordered SBA-15 mesoporous silica was demonstrated in a low cost, tube reactor without requiring mechanical or static mixers, using similar reagents and reaction conditions to those for conventional batch synthesis. Flow synthesis at 80 °C and 13 min residence time afforded SBA-15 with a BET surface of 566 m<sup>2</sup>.g<sup>-1</sup> (slightly lower than from batchwise synthesis) but a comparable pore volume, unit cell and well-defined (5.1 nm) mesopore channels, and with reduced complementary microporosity (advantageous for mass transport of bulky molecules). The yield and textural properties of flow synthesised SBA-15 was sensitive to reaction temperature and residence time, lower temperatures

and shorter times being detrimental to mesopore ordering (presumably due to slow silane hydrolysis/ poor micelle self-assembly), but insensitive to reactor operating time. SBA-15 productivity was greatly enhanced by flow operation, with a space-time yield (relative to the reactor volume) of 5.3 g.L<sup>-1</sup>.h<sup>-1</sup> versus 0.4-0.6 g.L<sup>-1</sup>.h<sup>-1</sup> for batch and alternative flow syntheses. Hydrothermal treatment of flow SBA-15 prior to calcination to remove the organic template conferred a modest increase in the surface area, total pore volume, and mesopore size, although these came at the expense of significantly lower productivity from the increased process time. Our simple reactor design offers a rapid and energy-efficient synthesis of SBA-15 and should be readily scalable for commercial production.

### **CRedit author statement**

Christopher M. A. Parlett; Conceptualization, Methodology, Data curation, Formal analysis, Investigation, Writing – original draft, Writing - review and editing. Hamidreza Arandiyani, Formal analysis, Writing – original draft, Writing - review and editing. Lee J. Durndell; Data curation. Mark A. Isaacs; Data curation, Writing - review and editing. Antonio Torres Lopez; Data curation. Roong J. Wong; Data curation. Karen Wilson; Conceptualization, Resources, Writing - review and editing. Adam F Lee; Conceptualization, Resources, Writing - review and editing.

### **Declaration of competing interests**

The authors declare that no known competing financial or personal interests may have influence the work reported.

### **Acknowledgment**

We thank the Australian Research Council for support (DP 200100204 and DP200100313). The authors would like to thank the Research Complex at Harwell and the UK Catalysis Hub for access and support to these facilities.

### **References**

1. C. T. Kresge, M. E. Leonowicz, W. J. Roth, J. C. Vartuli and J. S. Beck, *Nature*, 1992, **359**, 710-712.
2. Y. Wan and D. Y. Zhao, *Chem. Rev.*, 2007, **107**, 2821-2860.
3. T. Yasmin and K. Muller, *J. Chromatogr. A*, 2011, **1218**, 6464-6475.
4. V. F. Vavsari, G. M. Ziarani and A. Badiei, *RSC Adv.*, 2015, **5**, 91686-91707.
5. S. Sadjadi and M. M. Heravi, *RSC Adv.*, 2017, **7**, 30815-30838.
6. L. F. Giraldo, B. L. Lopez, L. Perez, S. Urrego, L. Sierra and M. Mesa, *Macromol. Symp.*, 2007, **258**, 129-141.
7. D. Y. Zhao, J. L. Feng, Q. S. Huo, N. Melosh, G. H. Fredrickson, B. F. Chmelka and G. D. Stucky, *Science*, 1998, **279**, 548-552.
8. T. Kjellman and V. Alfredsson, *Chem. Soc. Rev.*, 2013, **42**, 3777-3791.
9. J. L. Blin and M. Imperor-Clerc, *Chem. Soc. Rev.*, 2013, **42**, 4071-4082.
10. L. Cao, T. Man and M. Kruk, *Chem. Mat.*, 2009, **21**, 1144-1153.
11. D. Y. Zhao, J. Y. Sun, Q. Z. Li and G. D. Stucky, *Chem. Mat.*, 2000, **12**, 275-279.
12. M. Kruk, M. Jaroniec, C. H. Ko and R. Ryoo, *Chem. Mat.*, 2000, **12**, 1961-1968.
13. C. M. A. Parlett, A. Aydin, L. J. Durndell, L. Frattini, M. A. Isaacs, A. F. Lee, X. T. Liu, L. Olivi, R. Trofimovaite, K. Wilson and C. F. Wu, *Catal. Commun.*, 2017, **91**, 76-79.
14. C. M. A. Parlett, D. W. Bruce, N. S. Hondow, A. F. Lee and K. Wilson, *ACS Catal.*, 2011, **1**, 636-640.
15. M. Mesa, L. Sierra, B. Lopez, A. Ramirez and J. L. Guth, *Solid State Sci.*, 2003, **5**, 1303-1308.
16. D. Halamova, M. Badanicova, V. Zelenak, T. Gondova and U. Vainio, *Appl. Surf. Sci.*, 2010, **256**, 6489-6494.
17. M. A. Isaacs, B. Barbero, L. J. Durndell, A. C. Hilton, L. Olivi, C. M. A. Parlett, K. Wilson and A. F. Lee, *Antibiotics*, 2018, **7**, 55.
18. S. Y. Park and P. Pendleton, *Powder Technol.*, 2012, **223**, 77-82.
19. L. T. Gibson, *Chem. Soc. Rev.*, 2014, **43**, 5163-5172.

20. C. Chen, S. Zhang, K. H. Row and W. S. Ahn, *J. Energy Chem.*, 2017, **26**, 868-880.
21. S. V. Ley, *Chem. Rec.*, 2012, **12**, 378-390.
22. J. C. Pastre, D. L. Browne and S. V. Ley, *Chem. Soc. Rev.*, 2013, **42**, 8849-8869.
23. L. J. Durndell, M. A. Isaacs, C. E. Li, C. M. A. Parlett, K. Wilson and A. F. Lee, *ACS Catal.*, 2019, **9**, 5345-5352.
24. P. W. Dunne, A. S. Munn, C. L. Starkey, T. A. Huddle and E. H. Lester, *Philos. Trans. R. Soc. A-Math. Phys. Eng. Sci.*, 2015, **373**, 21.
25. M. Rubio-Martinez, C. Avci-Camur, A. W. Thornton, I. Imaz, D. MasPOCH and M. R. Hill, *Chem. Soc. Rev.*, 2017, **46**, 3453-3480.
26. Z. D. Liu, J. Zhu, T. Wakihara and T. Okubo, *Inorg. Chem. Front.*, 2019, **6**, 14-31.
27. S. C. Ryu, J. H. Lee and H. Moon, *Korean J. Chem. Eng.*, 2019, **36**, 1410-1416.
28. A. Sachse, A. Galarneau, F. Fajula, F. Di Renzo, P. Creux and B. Coq, *Microporous Mesoporous Mater.*, 2011, **140**, 58-68.
29. N. J. Hao, Y. Nie and J. X. J. Zhang, *ACS Sustain. Chem. Eng.*, 2018, **6**, 1522-1526.
30. N. J. Hao, Y. Nie, Z. Xu, A. B. Closson, T. Usherwood and J. X. J. Zhang, *Chem. Eng. J.*, 2019, **366**, 433-438.
31. C. L. Tong, R. A. Boulos, C. Z. Yu, K. S. Iyer and C. L. Raston, *RSC Adv.*, 2013, **3**, 18767-18770.
32. T. N. Ng, X. Q. Chen and K. L. Yeung, *RSC Adv.*, 2015, **5**, 13331-13340.
33. W. C. Jeong, M. Choi, C. H. Lim and S. M. Yang, *Lab Chip*, 2012, **12**, 5262-5271.
34. X. Q. Chen, M. Arruebo and K. L. Yeung, *Catal. Today*, 2013, **204**, 140-147.
35. J. Knossalla, S. Mezzavilla and F. Schuth, *New J. Chem.*, 2016, **40**, 4361-4366.
36. N. J. Hao, Y. Nie, A. Tadimety, A. B. Closson and J. X. J. Zhang, *Mater. Res. Lett.*, 2017, **5**, 584-590.
37. N. J. Hao, Y. Nie, A. B. Closson and J. X. J. Zhang, *J. Colloid Interface Sci.*, 2019, **539**, 87-94.
38. A. B. Corradi, F. Bondioli, A. M. Ferrari, B. Focher and C. Leonelli, *Powder Technol.*, 2006, **167**, 45-48.
39. S. Komarneni, R. Roy and Q. H. Li, *Mater. Res. Bull.*, 1992, **27**, 1393-1405.
40. S. Fei, Y. Zhang, J. Zhang, Z. Tang and Q. Wu, *J. Flow Chem.*, 2021, DOI: 10.1007/s41981-021-00157-2.
41. W. Stöber, A. Fink and E. Bohn, *J. Colloid Interface Sci.*, 1968, **26**, 62-69.
42. J. Jammaer, A. Aerts, J. D'Haen, J. W. Seo and J. A. Martens, *J. Mater. Chem.*, 2009, **19**, 8290-8293.
43. J. Jammaer, T. S. van Erp, A. Aerts, C. E. A. Kirschhock and J. A. Martens, *J. Am. Chem. Soc.*, 2011, **133**, 13737-13745.
44. M. G. Colmenares, U. Simon, O. Cruz, A. Thomas, O. Goerke and A. Gurlo, *Microporous Mesoporous Mater.*, 2018, **256**, 102-110.
45. D. Y. Zhao, Q. S. Huo, J. L. Feng, B. F. Chmelka and G. D. Stucky, *J. Am. Chem. Soc.*, 1998, **120**, 6024-6036.
46. M. Thommes, K. Kaneko, A. V. Neimark, J. P. Olivier, F. Rodriguez-Reinoso, J. Rouquerol and K. S. W. Sing, *Pure Appl. Chem.*, 2015, **87**, 1051-1069.
47. X. L. Ji, K. T. Lee, M. Monjauze and L. F. Nazar, *Chem. Commun.*, 2008, DOI: 10.1039/b804327b, 4288-4290.
48. S. G. Wainwright, C. M. A. Parlett, R. A. Blackley, W. Zhou, A. F. Lee, K. Wilson and D. W. Bruce, *Microporous Mesoporous Mater.*, 2013, **172**, 112-117.
49. E. Rammerstorfer, T. Karner and M. Siebenhofer, *Heat Trans. Eng.*, 2020, **41**, 691-707.
50. S. Fries, D. M. Castañeda-Zúñiga, J. Duchateau, P. Neuteboom, C. T. Porras and M. Busch, *Macromol. Symp.*, 2016, **360**, 78-86.
51. X. Ni, M. R. Mackley, A. P. Harvey, P. Stonestreet, M. H. I. Baird and N. V. Rama Rao, *Chem. Eng. Res. Des.*, 2003, **81**, 373-383.
52. Q. S. Huo, D. I. Margolese and G. D. Stucky, *Chem. Mat.*, 1996, **8**, 1147-1160.
53. T. J. Rottreau, C. M. A. Parlett, A. F. Lee and R. Evans, *Microporous Mesoporous Mater.*, 2018, **264**, 265-271.